

# Using spin bias to manipulate and measure spin in quantum dots

Hai-Zhou Lu<sup>1</sup> and Shun-Qing Shen<sup>1</sup>

<sup>1</sup>*Department of Physics, and Centre of Theoretical and Computational Physics,  
The University of Hong Kong, Pokfulam Road, Hong Kong, China*

(Dated: November 10, 2018)

A double quantum dot coupled to electrodes with spin-dependent splitting of chemical potentials (spin bias) is investigated theoretically by means of the nonequilibrium Keldysh Green's function formalism. By applying a large spin bias, the quantum spin in a quantum dot (dot 1) can be manipulated in a fully electrical manner. To noninvasively monitor the manipulation of the quantum spin in dot 1, it is proposed that the second quantum dot (dot 2) is weakly coupled to dot 1. In the presence of the exchange interaction between the two dots, the polarized spin in dot 1 behaves like an effective magnetic field and weakly polarizes the spin in the nearby quantum dot 2. By applying a very small spin bias to dot 2, the spin-dependent transport through dot 2 can be probed, allowing the spin polarization in dot 1 to be identified nondestructively. These two steps form a complete scheme to manipulate a trapped spin while permitting this manipulation to be monitored in the double-dot system using pure electric approaches.

PACS numbers: 85.75.-d, 73.21.La, 72.25.Hg

## I. INTRODUCTION

The manipulation and measurement of single electron spin in a quantum dot is the basis toward scalable spin-based quantum information processing.<sup>1</sup> The preparation and readout of a single spin in a quantum dot have been demonstrated using photoluminescence polarization<sup>2,3</sup> and polarization-dependent absorption.<sup>4,5,6</sup> The rapid progress of the charging sensing technique<sup>7,8</sup> makes it possible to control the number of electrons inside quantum dots precisely down to a few electrons,<sup>9</sup> allowing an individual electron spin to be manipulated with the help of stationary and oscillating electromagnetic field,<sup>10,11</sup> and the readout by various spin-to-charge conversion techniques, such as single-shot readout using energy<sup>12</sup> or tunneling rate difference<sup>13</sup> and Pauli spin blockade.<sup>10</sup> However, most of the detection techniques destroy the originally prepared spin state. All the electric approaches remove the trapped spin from its host dot, and most of optical measurements drive the spin polarized states to other states. A noninvasive detection method is needed because a complete control process requires the manipulated spin to be monitored and not be affected by the monitoring. Recently, using off-resonant picosecond-scale optical pulses and time-resolved Kerr rotation spectroscopy, single electron spin in a quantum dot is nondestructively measured,<sup>14</sup> which further leads to better manipulation of the spin.<sup>15</sup> Besides, by using energy-dependent single-shot readout followed by immediate restoring of the spin back to dot within a time shorter than the spin relaxation time, up to 90% of the original spin states can be retained after the measurement.<sup>16</sup> Still, all the techniques require precisely controlled gating, electromagnetic or optical field, and their time scale has to be within the spin coherence time considering various decoherence mechanisms in host materials.

A hint from the charging sensing technique<sup>7,8</sup> is that it makes use of a nearby quantum point contact to noninvasively measure the electron number in the quantum dot, which avoids destroying the electron occupation in the quantum dot by direct transport measurement. From the point of view of spin-

based quantum information processing, it would be highly desirable to design a similar device with integrated ability to manipulate a trapped single spin while permitting the manipulation to be read out nondestructively in quantum dot. Most importantly, a pure electric approach (in the absence of magnetic or optical field) is particularly appealing for a large-scale integration.

A possible direction for this effort points to the spin injection technique, i.e., generating a nonequilibrium spin accumulation in nonmagnetic (paramagnetic) materials, which could induce a spin-dependent splitting of chemical potentials or spin bias in the injected materials. Spin injection has been demonstrated using several of electric and optical approaches. One of the effective methods is to inject spin-polarized charge current directly from ferromagnetic to nonmagnetic materials.<sup>17</sup> The unequal density of states for majority and minority spins at the Fermi level of the ferromagnet will induce a spin accumulation in the nonmagnetic material and split the chemical potentials for two spin components. The materials and geometries used in this method include metals,<sup>18,19,20</sup> metal/barrier/semiconductors,<sup>21,22,23</sup> and ferromagnetic/normal semiconductors.<sup>24,25</sup> In the last few years, spin injection has also been shown by means of the spin Hall effect<sup>26,27</sup> and the incidence of linearly or circularly polarized light into a two-dimensional electron gas with spin-orbital coupling.<sup>28,29,30</sup> Notice that many of the intensively investigated spin-injected nonmagnetic materials are also widely used to fabricate electrodes probing semiconductor<sup>31</sup> and single-molecule quantum dots.<sup>32</sup> Therefore, it is interesting to investigate the polarization and detection of electron spin in quantum dot systems using electrodes with spin bias. Experimentally, spin injection into all-semiconductor quantum dots has been reported, from (Ga,Mn)As to InAs quantum dots (QDs)<sup>33</sup>, and from BeMnZnSe to a single CdSe/ZnSe QD, both combined with a spin-light-emitting-diode to detect spin polarization. Furthermore, several theoretical works addressed the transport through mesoscopic systems in the presence of spin-splitting of chemical potentials.<sup>34,35,36,37</sup>

Motivated by these experimental and theoretical progresses,

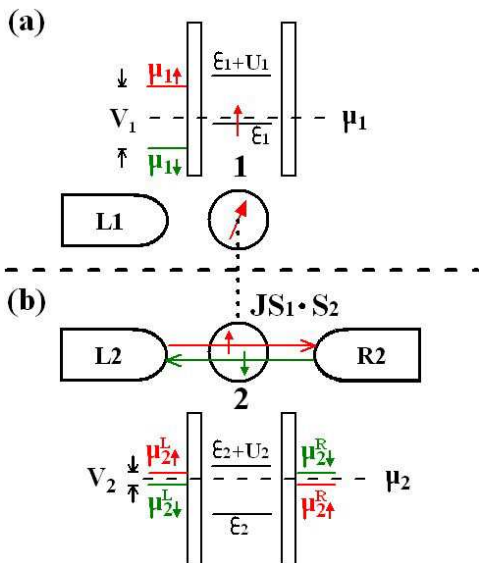


FIG. 1: Schematic of our double-dot system, in which each dot is attached to its own electrodes with spin-dependent splitting of chemical potentials (spin biases). (a) A large spin bias  $V_1$  is applied to manipulate the quantum spin in dot 1. The energy zero point is set at  $\epsilon_1 + U_1/2$ . The spin bias  $V_1$  induces a splitting of the Fermi levels for  $\uparrow$  and  $\downarrow$  electrons in lead L1 so that  $\mu_{1\uparrow/\downarrow} = \mu_1 \pm V_1/2$ , where  $\mu_1$  is the middle point of the Fermi levels. (b) Due to the exchange interaction between the two dots, the polarized spin in dot 1 behaves like an effective magnetic field and weakly polarizes the spin in dot 2. A very small spin bias  $V_2$  is applied to the dot 2 to probe its spin-dependent transport, allowing the spin polarization in dot 1 to be read out nondestructively.  $\mu_2$  is the equilibrium Fermi level for both leads L2 and R2. The spin bias  $V_2$  induces a splitting of the Fermi levels for  $\uparrow$  ( $\downarrow$ ) electrons in the leads of dot 2, so that  $\mu_{2\uparrow/\downarrow}^L = \mu_2 \pm V_2/2$  and  $\mu_{2\uparrow/\downarrow}^R = \mu_2 \mp V_2/2$ .

we propose a scheme to realize the control and detection of quantum spin in semiconductor quantum dot by using spin bias or spin current. Our setup consists of a double-quantum-dot system connected to electrodes as shown in Fig. 1. A quantum spin state can be generated and maintained in dot 1 when applying a spin bias  $V_1$  on the electrode coupling the quantum dot 1 [Fig. 1(a)]. In the presence of exchange interaction between the two dots, the polarized spin in dot 1 behaves like an effective magnetic field and breaks the spin symmetry in dot 2. As a result, it will induce a charge current when a small spin bias  $V_2$  is applied or a spin current flows through dot 2, allowing the spin polarization in dot 1 to be identified [Fig. 1 (b)]. If the interdot exchange interaction is much smaller than  $V_1$ , the measurement can be viewed as non-destructive. These two steps form a complete scheme of manipulating and measuring the quantum spin state of a trapped electron in one dot of a double-dot system using purely electric means. Our proposal is based on steady-state evaluation; no ultrafast optical or electrostatic operation is needed. We argue that it is robust once the magnitude of  $V_1$  energetically overwhelms those of decoherence mechanisms, such as hyperfine interaction with nuclear spins of host materials, or spin-orbital coupling. It is worth stressing that as the spin injection

techniques of various means are still under extensive investigations and progress, in the present work, we focus only on the physical consequences of spin bias or spin current, and ignore the approaches to generate the spin bias at the current stage.

The present paper is organized as follows: In Sec. II, we present the general scheme and description of the manipulation and detection of a single spin using the idea of spin bias, by comparing with the known charge sensing technique. The model Hamiltonian is introduced. The experimental feasibility of our scheme is discussed based on recent experimental availability. In Sec. III, the manipulation of quantum spin in dot 1 is addressed. The stability diagrams of electron number and spin polarization in dot 1 are presented. In Sec. IV, the measurement of the spin polarization in the dot 1 using the spin-dependent transport through dot 2 is discussed. A detailed analytical calculation and the numerical results are presented. We focus on the charge current induced by the spin bias or spin conductance through dot 2 and its relation with the spin polarization in dot 1. In Sec. V, a summary is presented. Finally, the detailed calculations of spin conductance and Green's functions are presented in Appendices A and B for reference.

## II. GENERAL PROPOSAL

### A. Spin sensing scheme

A typical setup for charge sensing technique (sketched in the second column of Table I) consists of a quantum dot which hosts the electrons to be manipulated and a nearby quantum point contact.<sup>7</sup> The electron number inside the host dot can be determined by directly probing the transport through dot; however, this approach implies removing electrons from dot, destroying the original occupation. Alternatively, due to Coulomb repulsion, the transport through the quantum point contact is found to be very sensitive to the electron number in dot and thus can be used to determine the electron number. Most importantly, this approach is noninvasive because it does not change the electron number in dot.

Our scheme combining spin manipulation and detection in one setup employs a similar idea. We apply the electron spin to play the role of the electron charge in the device. As shown in Fig. 1, the setup is composed of two quantum dots. dot 1 is the host for the manipulated spin. dot 2 is used to non-destructively detect the spin in dot 1, analogous to the function of quantum point contact in charge sensing. Each dot is coupled independently to its nonmagnetic leads. The Fermi levels of the leads are spin dependent and can be split by the spin bias. Without loss of generality, we consider only one spin-degenerate energy level in each dot, denoted as  $\epsilon_i$  for a dot  $i$  ( $i = 1, 2$ ). The two dots are assumed to be coupled weakly to each other via the Heisenberg exchange coupling with strength  $J$ .

To manipulate the spin in dot 1, we apply a spin bias  $V_1$  to lead L1 attached to dot 1. To retain the electrons in dot 1, we consider only one reservoir to avoid electron transport in the

usual two-reservoir case. We denote by  $\mu_{1\sigma}$  the Fermi level for  $\sigma$  electrons in lead L1. The spin bias  $V_1$  induces a splitting of the Fermi levels for spin  $\uparrow$  and  $\downarrow$  electrons in lead L1 so that

$$\begin{aligned}\mu_{1\uparrow} &= \mu_1 + V_1/2, \\ \mu_{1\downarrow} &= \mu_1 - V_1/2,\end{aligned}$$

where  $\mu_1$  is the middle point of the Fermi levels,

$$\mu_1 = \frac{1}{2}(\mu_{1\uparrow} + \mu_{1\downarrow}),$$

which can be tuned with respect to  $\epsilon_1$  by using the gate voltage. The energy zero point is set at  $\epsilon_1 + U_1/2$ . When the dot 1 is coupled to its reservoir, the electron number inside it at low temperatures will be determined by the relative location between dot level  $\epsilon_1$  and the Fermi levels of the reservoir. In the absence of spin-dependent splitting of chemical potentials ( $\mu_{1\uparrow} = \mu_{1\downarrow}$ ), it is known that dot will be filled or empty when the Fermi levels are well above or below dot level. Similarly, in the presence of the spin-resolved Fermi levels, the filling of spin  $\uparrow$  ( $\downarrow$ ) electron in dot 1 is determined independently by the relative location between  $\epsilon_1$  and  $\mu_{1\uparrow}$  ( $\mu_{1\downarrow}$ ). The simplest situation, shown in Fig. 1, is that when  $\mu_{1\downarrow} < \epsilon_1 < \mu_{1\uparrow}$ , only  $\uparrow$  electron is energetically allowed to stay in dot; therefore, the electron spin in dot is  $\uparrow$  polarized. When considering the on-site Coulomb repulsion, detailed calculations are required; these are presented in Sec. III.

In the presence of exchange interaction, once the electron in dot 1 is polarized by  $V_1$ , it will act approximately as an effective magnetic field and weakly polarize the electron in the nearby dot 2. The polarized spin in dot 2 will, in turn, act as an effective magnetic field to dot 1 and will influence the polarization of dot 1. If there is no extra mechanism to break the spin symmetry, this self-consistent process repeats until  $\langle s_1^z \rangle$  and  $\langle s_2^z \rangle$  approach zero, where  $\langle s_i^z \rangle \equiv \frac{1}{2}(\langle n_{i\uparrow} \rangle - \langle n_{i\downarrow} \rangle)$  is the spin polarization in dot  $i$  and  $\langle n_{i\sigma} \rangle$  is the electron occupation for spin- $\sigma$  electron in dot  $i$ . However, in the limit

$$V_1 \gg J \langle s_2^z \rangle, \quad (1)$$

the spin polarization in dot 1 is dominantly determined by the spin bias  $V_1$  and is hardly affected by the effective magnetic field generated by dot 2. Once the spin is polarized in dot 1, it imposes a selection rule to the spin orientation of electrons that can tunnel through dot 2 because the ground state of the two spins that are singly occupied in each dot tends to form a fixed alignment in the presence of the exchange interaction. Therefore, by measuring the spin polarization of the current that can flow through dot 2, the spin orientation of dot 1 can be read out. Because of Eq. (1), this measurement can be viewed as nondestructive.

To measure the spin-polarization of the current that can flow through the dot 2, a small spin bias  $V_2$  is applied to the electrodes attached to the dot 2 so that the Fermi levels split in the left lead,

$$\mu_{2\uparrow/\downarrow}^L = \mu_2 \pm V_2/2,$$

and in the right lead,

$$\mu_{2\uparrow/\downarrow}^R = \mu_2 \mp V_2/2,$$

where  $\mu_2$  is the Fermi level when there is no spin and charge biases. Notice that in the presence of the pure spin bias  $V_2$ , electrons of spin  $\uparrow$  and  $\downarrow$  will flow along opposite directions through dot 2. In our definition, the spin- $\uparrow$ ( $\downarrow$ ) current can only flow from the left (right) to the right (left). If the up-down symmetry of the electron spin in dot is not broken, electric currents of spin  $\uparrow$  and  $\downarrow$  will cancel each other. Consequently a pure spin current is formed.<sup>38</sup> However, if the spin symmetry of dot 2 is broken, the pure spin bias  $V_2$  applied to the dot 2 will generate a net electric current. In this way, measuring the direction of current through dot 2 in the presence of  $V_2$  is enough to determine the spin polarization of the current through dot 2 and the spin orientation in dot 1. Furthermore, to avoid the polarization of the spin in dot 2 affected by  $V_2$ , we demand that

$$J \langle s_1^z \rangle \gg V_2. \quad (2)$$

## B. Model for coupled double dot

The Hamiltonian for the whole double-dot consists of three parts,

$$H = H_1 + H_2 + V_{12}, \quad (3)$$

where  $H_i$  is the Hamiltonian for a dot  $i$  and its leads alone, described by the Anderson model,<sup>39</sup>

$$\begin{aligned}H_i &= \sum_{\sigma} \epsilon_i n_{i\sigma} + U_i n_{i\uparrow} n_{i\downarrow} + \sum_{k,\sigma} \epsilon_{k\alpha\sigma} c_{k\alpha\sigma}^{\dagger} c_{k\alpha\sigma} \\ &+ \sum_{k,\sigma} (V_{k\alpha\sigma} c_{k\alpha\sigma}^{\dagger} d_{i\sigma} + h.c.),\end{aligned} \quad (4)$$

where  $d_{i\sigma}^{\dagger}$  ( $d_{i\sigma}$ ) represents the creation (annihilation) operator for the discrete state with energy  $\epsilon_i$  and spin  $\sigma$  ( $\in \{\uparrow, \downarrow\}$ ) in dot  $i$ , the number operator  $n_{i\sigma} = d_{i\sigma}^{\dagger} d_{i\sigma}$ , and  $U_i$  is the intra-dot Coulomb repulsion.  $c_{k\alpha\sigma}^{\dagger}$  ( $c_{k\alpha\sigma}$ ) is the creation (annihilation) operator for a continuous state in the  $\alpha$  lead (reservoir) with energy  $\epsilon_{k\alpha\sigma}$  and spin  $\sigma$ . The tunneling matrix element  $V_{k\alpha\sigma}$  is assumed to be independent of  $k$  in the following calculations.

$V_{12}$  in Eq. (3) stands for the interaction between the two dots. Basically, there are three forms of interactions:

(1) The tunneling coupling ( $t_c d_{1\sigma}^{\dagger} d_{2\sigma} + h.c.$ ).<sup>40</sup> When the two dots are very closely located electrons are allowed to tunnel between the two dots directly. It should be avoided if one intends to perform a noninvasive measurement. We will discuss how to prevent it in Sec. II C.

(2) The capacitive coupling  $U' n_1 n_2$ .<sup>41</sup> The Coulomb repulsive interaction always exists when the two dots are closely located, but well separated. The occupancy of electrons in one dot will affect the charge transport in the other dot. This is the microscopic mechanism for the charge sensing technique. However it is not spin-resolved, and we shall ignore it in our calculation. We will explain in Sec. IV C that neglecting this term brings no qualitatively change.

(3) The Heisenberg exchange coupling,

$$V_{12} = J \mathbf{s}_1 \cdot \mathbf{s}_2 \quad (5)$$

where  $\mathbf{s}_i = \frac{1}{2} \sum_{\sigma, \sigma'} d_{i\sigma}^\dagger \hat{\sigma}_{\sigma\sigma'} d_{i\sigma'}$  and  $\hat{\sigma} = (\sigma_x, \sigma_y, \sigma_z)$  are the Pauli matrices.<sup>42</sup> It does not change the occupation number of each dot; but it affects the states of electron spin, in particular, when the electrons are spin resolved. To simplify our calculation, we consider only the exchange coupling.

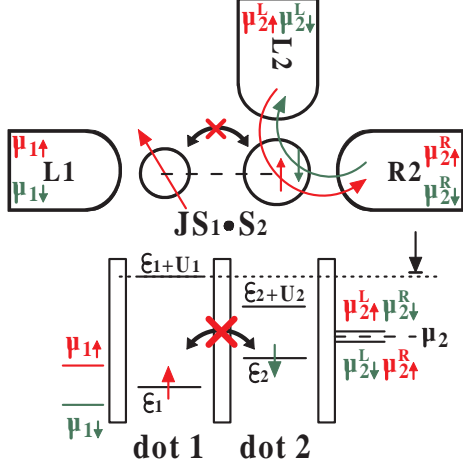


FIG. 2: Schematic and energy configuration of the low-energy effective double-dot model. The interdot first-order direct tunneling is suppressed due to careful design of all characteristic energies. The second-order virtual hopping induces a low-energy Heisenberg exchange interaction with a considerable positive exchange strength  $J$ .  $\mu_{2\sigma}^\alpha$  is the Fermi level for spin  $\sigma (\in \{\uparrow, \downarrow\})$  electrons in the  $\alpha (\in \{L2, R2\})$  lead of dot 2.  $\mu_2 = \frac{1}{2}(\mu_{2\uparrow}^{L/R} + \mu_{2\downarrow}^{L/R})$  is the shared middle point of Fermi levels for both leads L2 and R2.

### C. Experimental feasibility

We have to point out that the model in Eqs. (3) and (5) with considerable  $J$  is valid in experiments only as a low-energy effective Hamiltonian when direct electron hopping is quenched between two tunneling-coupled quantum dots (coupling constant  $t_c$  can be as large as hundreds of  $\mu\text{eV}$ ).<sup>42,43</sup> To suppress the direct tunneling and to employ only the low-energy spin dynamics between the two dots, the energy configuration of the double dot should be carefully designed, as shown in Fig. 2. The level energies of the two dots can be adjusted with respect to each other by tuning the gate voltages, while the charging energies of the two dots can be customized by engineering the dot sizes.<sup>42</sup> We choose an energy configuration such that  $\epsilon_2 - \epsilon_1 > |t_c|$  and  $(\epsilon_1 + U_1) - (\epsilon_2 + U_2) > |t_c|$ . For dot 1,  $\mu_1$  and  $V_1$  are restricted to the singly occupied regimes shown in Fig. 3. Moreover, since  $\epsilon_1 < \epsilon_2$ , the electron in dot 1, which resides on  $\epsilon_1$ , cannot hop to dot 2 no matter whether dot 2 is occupied or not. For dot 2, the scanning range of the middle point of the Fermi level  $\mu_2$  is well restricted,  $< \epsilon_1 + U_1$  (as shown by dotted line in Fig. 2). As a result, although double occupation in dot 2 is allowed when  $\mu_2 > \epsilon_2 + U_2$ , the electrons in dot 2 still cannot hop to dot 1 because they can not acquire enough energy from  $\mu_{2\sigma}^\alpha$  to conquer the charging

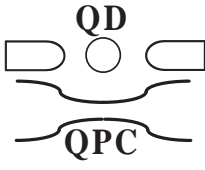
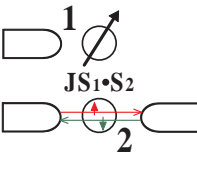
energy  $U_1$  for double occupation in dot 1. The above conditions assure that there is no direct hopping between the two dots. However, due to the uncertainty principle, within a time  $\sim \hbar/U_i$  or  $\sim \hbar/|\epsilon_1 - \epsilon_2|$ , an electron in dot 1 (2) can still possibly hop to dot 2 (1) and back. Because of the Pauli exclusion principle, this kind of second-order virtual hopping favors the anti-parallel alignment of two spins in the double dot. As a result, the low-energy correlation between the two dots is well described by the Heisenberg Hamiltonian with a positive exchange coupling strength  $J$ . Using the simplest Hubbard model estimate  $J = \frac{4t_c^2}{U}$ ,  $J$  can be as large as 0.09 meV when  $t_c = 0.15$  meV and  $U \sim 1$  meV.<sup>42</sup>

In addition, we have to consider the experimental possibilities for the requirements in Eqs. (1) and (2). Generally,  $\langle s_z^2 \rangle$  must be within  $[-0.5, 0.5]$  (as shown in Fig. 6;  $|\langle s_z^2 \rangle|$  is actually less than 0.2 in our results). According to the experiment based on a semiconductor QD,<sup>42</sup>  $J \sim 0.09$  meV, so the order of the spin biases  $V_1$  required for the manipulation should  $\gg 0.045$  meV, which should be within reach of the experiments. For example, Zaffalon and van Wees<sup>44</sup> reported that the spin-polarized current injected from Co electrodes to an Al island induces a splitting  $\mu_\uparrow - \mu_\downarrow = eIR_s/P$ , where  $I \sim 10 - 100 \mu\text{A}$  is the injection current,  $P = 7\%$  is the spin injection efficiency of the Co/Al tunnel barrier, and  $R_s$  is a defined quantity of the dimension of resistance, which was measured up to 250 m $\Omega$  at 4.2 K. Therefore, the spin bias in this experiment can be as large as  $e \times 0.1 \text{ mA} \times 250 \text{ m}\Omega / 0.07 \sim 0.35$  meV. Although it is not explicitly addressed in publications<sup>21,22,23,26,27,45</sup> to our knowledge, the values of the spin-dependent chemical potential splitting in semiconductors may be larger than those in metals, based on the following two arguments: First, the density of states near the Fermi level is much smaller in semiconductors. The same imbalance of one spin component compared to that of the other should occupy a wider range of energy. Second, the measured spin diffusion lengths in semiconductors are usually  $\sim 1 - 10 \mu\text{m}$ ,<sup>45</sup> much longer than those in metals ( $\sim$  hundreds of nanometers),<sup>46</sup> so the spin accumulation in semiconductors are more robust in maintaining a considerable spin bias. For Eq. (2),  $V_2$  should be, of course, as small as possible, while the only low bound for  $V_2$  is that it should be large enough to generate measurable current. The current measured in a QD experiment can be as small as  $\Delta I \sim \text{pA}$  (47) to our knowledge, while the conductance through a quantum dot is on the order of  $\frac{2e^2}{h} \approx 7.75 \times 10^{-5} \Omega^{-1}$ . Thus, the minimum bias voltage required to generate such a small current is on the order of  $\Delta I / \frac{2e^2}{h} = \text{pA} / (7.75 \times 10^{-5} \Omega^{-1}) \sim \mu\text{V}$ , which is orders of magnitude smaller than the reported value of  $J \sim 90 \mu\text{eV}$  estimated in the experiment.<sup>42</sup>

Throughout this work, the temperature is assumed to be the smallest one among all physical quantities. According to the experiment,<sup>42</sup> we choose  $k_B T = 4 \mu\text{eV}$  in the following calculations.

For a brief summary, we compare our spin sensing scheme with the charge sensing technique in Table. I.

TABLE I: Comparison between charge sensing technique and spin sensing technique in the present work.

	Charge sensing <sup>7,8</sup>	Our model
Configuration		
Quantity manipulated and detected (Range)	Electron number in QD (0,1,2...)	Single spin in QD1 (-0.5 ~ 0.5)
Manipulation approach	Tuning gate voltage of QD	Applying large spin bias to QD1
Interaction	Coulomb repulsion	Exchange interaction $J\mathbf{s}_1 \cdot \mathbf{s}_2$
Detector	QPC	QD2
Measured quantity in detector	Charge conductance by applying charge bias	Spin conductance by applying spin bias

### III. MANIPULATION OF QUANTUM SPIN BY MEANS OF SPIN BIAS

In this section, we present the calculation and numerical results of the first part of our scheme, the manipulation of the spin in dot 1. Based on the agreement in the Sec. II C, It is safe and convenient to ignore dot 2 and the spin correlation between dots 1 and 2 in this section.

#### A. Spin polarization and Green's function technique

In order to determine the optimal parameters to polarize a single spin, we calculate the polarization of the electron spin  $\langle s_1^z \rangle = (\langle n_{1\uparrow} \rangle - \langle n_{1\downarrow} \rangle)/2$  and the total electron number  $\langle n_1 \rangle = \langle n_{1\uparrow} \rangle + \langle n_{1\downarrow} \rangle$  in dot 1 as functions of the spin bias  $V_1$  and the middle point  $\mu_1$  of the Fermi level. The formula for the  $\sigma$  component of particle number  $\langle n_{1\sigma} \rangle$  can be expressed in terms of the lesser Green's function,<sup>48,49</sup>

$$\langle n_{1\sigma} \rangle = -i \int \frac{d\omega}{2\pi} G_{1\sigma}^<(\omega),$$

where

$$G_{1\sigma}^< = G_{1\sigma}^r \Sigma_{1\sigma}^< [G_{1\sigma}^r]^\dagger, \quad \Sigma_{1\sigma}^< = i\Gamma_1 f_{1\sigma},$$

where  $G_{1\sigma}^r(\omega)$  are the retarded Green's functions defined as the Fourier transform of  $G_{1\sigma}^r(t) = -i\theta(t)\langle \{d_{1\sigma}(t), d_{1\sigma}^\dagger\} \rangle$ , where  $d_{1\sigma}(t) = e^{iH_1 t} d_{1\sigma} e^{-iH_1 t}$ .  $\Gamma_1 = \sum_k 2\pi |V_{k\sigma}|^2 2\pi\delta(\omega - \epsilon_{k\sigma})$  is the broadening of the quantum dot level  $\epsilon_1$ , due to its coupling to lead L1 for  $\uparrow$  or  $\downarrow$  electrons.  $\Gamma_1$  is assumed to be independent of  $\sigma$  since we are not addressing a ferromagnetic electrode.

$f_{1\sigma}$  is the Fermi-Dirac distribution of  $\sigma$  electrons in the lead,

$$f_{1\sigma}(\omega) = \frac{1}{e^{(\omega - \mu_{1\sigma})/k_B T} + 1},$$

where  $T$  is the temperature and  $k_B$  is the Boltzmann constant. Up to the second-order of Hartree-Fock approximation, the retarded Green's function of dot 1 is given by<sup>48</sup>

$$G_{1\sigma}^r = \frac{1 - \langle n_{1\bar{\sigma}} \rangle}{\omega - \epsilon_1 + \frac{i}{2}\Gamma_1} + \frac{\langle n_{1\bar{\sigma}} \rangle}{\omega - \epsilon_1 - U_1 + \frac{i}{2}\Gamma_1}.$$

Here we do not consider the Kondo effect in dot because it is usually suppressed due to the large spin bias  $V_1$ .

#### B. Numerical results

The electron number  $\langle n_1 \rangle$  and spin-polarization  $\langle s_1^z \rangle$  diagrams are shown in Fig. 3 as functions of the pure spin bias  $V_1$  and the Fermi level middle point  $\mu_1$ . In the calculations, we choose a set of typical parameters  $k_B T = 0.004$  meV,  $U_1 = 1.2$  meV, and  $\Gamma_1 = 0.0375$  meV, in accordance with the experiment.<sup>42</sup>  $\epsilon_1 = -0.6$  meV to assure that  $\epsilon_1 + U_1/2$  is the energy zero point.

As shown in Fig. 3, when the spin bias  $V_1 = 0$ , the electron number will be 0, 1, and 2 if  $\mu_1$  is well below  $\epsilon_1$ , between  $[\epsilon_1, \epsilon_1 + U_1]$ , and above  $\epsilon_1 + U_1$ , respectively. The empty, singly occupied, and doubly occupied unpolarized regimes are denoted by **E0**, **S0**, and **D0**, respectively. Each regime develops into two spin-polarized regimes when a positive ( $V_1 > 0$ ) or negative ( $V_1 < 0$ ) spin bias is applied. **E0**  $\rightarrow$  **S $\uparrow$ 1**, **S $\downarrow$ 1**; **S0**  $\rightarrow$  **S $\uparrow$ 2**, **S $\downarrow$ 2**; and **D0**  $\rightarrow$  **S $\uparrow$ 3**, **S $\downarrow$ 3**. We denote the nine regimes by the electron number and polarization. 0,  $\uparrow$ , and  $\downarrow$  stand for unpolarized, spin up, and spin down, respectively. For example, **S $\uparrow$ 2** represents the second regime when dot 1 is singly occupied and  $\uparrow$  polarized. We describe the nine regimes one by one as follows:

(1) **E0**: Both  $\mu_{1\uparrow}$  and  $\mu_{1\downarrow}$  are well below  $\epsilon_1$ ; the dot is then empty and unpolarized.

(2) **S $\uparrow$ 1**: This is obtained by applying a positive spin bias to **E0** until  $\mu_{1\uparrow}$  is above  $\epsilon_1$ , while  $\mu_{1\downarrow}$  is still below  $\epsilon_1$ , so only an electron of spin up is energetically allowed to occupy dot. The spin in dot 1 is  $\uparrow$  polarized.

(3) **S $\downarrow$ 1**: This is opposite to **S $\uparrow$ 1** and is obtained by applying a negative spin bias.

(4) **S0**: Both  $\mu_{1\uparrow}$  and  $\mu_{1\downarrow}$  are between  $\epsilon_1$  and  $\epsilon_1 + U_1$ . At least one electron can be filled into dot. However, neither  $\mu_{1\uparrow}$  nor  $\mu_{1\downarrow}$  can compensate for the charge energy  $U_1$  for filling the second electron. The opportunity of occupation for spin-up or spin-down electron is the same. Therefore, the electron spin is unpolarized.

(5) **S $\uparrow$ 2**: This is obtained by applying a positive spin bias to **S0** until  $\mu_{1\downarrow}$  is well below  $\epsilon_1$  or  $\mu_{1\uparrow}$  is well above  $\epsilon_1 + U_1$ . The former situation is similar to **S $\uparrow$ 1**. In the latter situation, if dot is initially occupied by a  $\downarrow$  spin, an  $\uparrow$  spin can still enter dot because  $\mu_{1\uparrow} > \epsilon_1 + U_1$ . Once the  $\uparrow$  spin enters the dot, the  $\downarrow$  spin will be repulsed out of dot and unable to enter again because  $\mu_{1\downarrow} < \epsilon_1 + U_1$  cannot supply enough charge energy. Both situations lead to a spin  $\uparrow$  electron filled in dot.



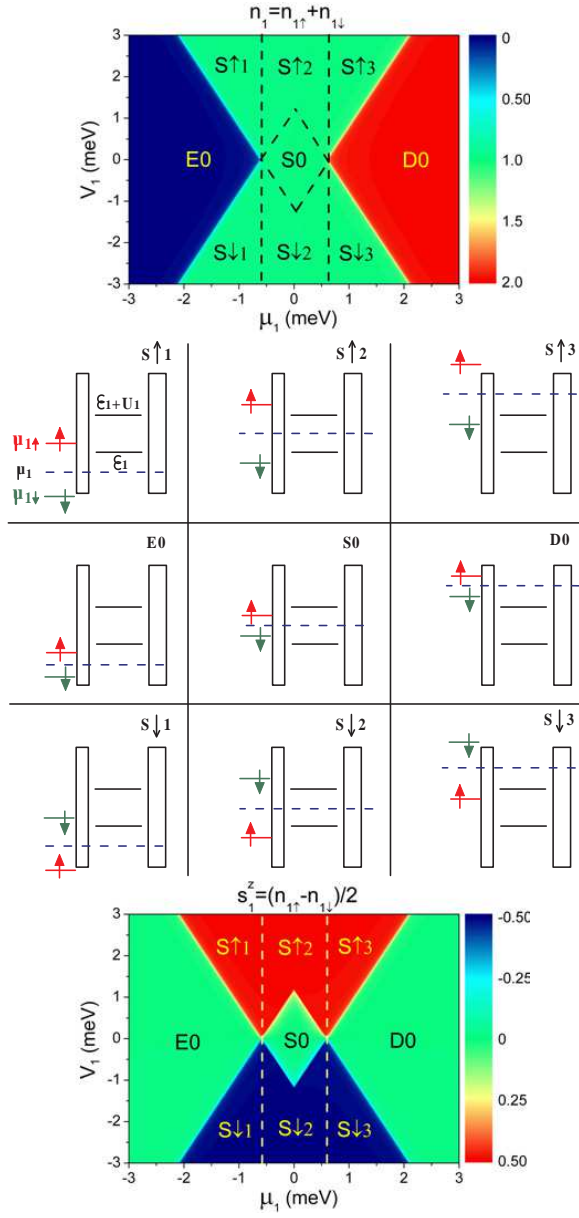


FIG. 3: The total electron number  $\langle n_1 \rangle$  (top panel) and spin polarization  $\langle s_1^z \rangle$  (bottom panel) diagrams as functions of the spin bias  $V_1$  and the Fermi level middle point  $\mu_1$ . The diagrams can be divided into nice configurations, schematically shown in the middle panel, starting from three unpolarized states **E0**, **S0**, and **D0** with electron numbers  $n_1 = 0, 1, 2$ , respectively. **E**=empty, **S**=singly-occupied, **D**=doubly-occupied; and  $0, \uparrow$ , and  $\downarrow$  represent unpolarized and two polarized states.

(6) **S↓2**: This is opposite to **S↑2** and is obtained by applying a negative spin bias.

(7) **D0**: Both  $\mu_{1\uparrow}$  and  $\mu_{1\downarrow}$  are well above  $\epsilon_1 + U_1$ ; dot is occupied by two electrons, one up and the other down due to the Pauli exclusive principle. Thus, there is no polarization.

(8) **S↑3**:  $\mu_{1\uparrow}$  is well above  $\epsilon_1 + U_1$ , while  $\mu_{1\downarrow}$  is below  $\epsilon_1 + U_1$ .

(9) **S↓3**: This is opposite to **S↑3**.

As shown in Fig. 3, the edges between different regimes

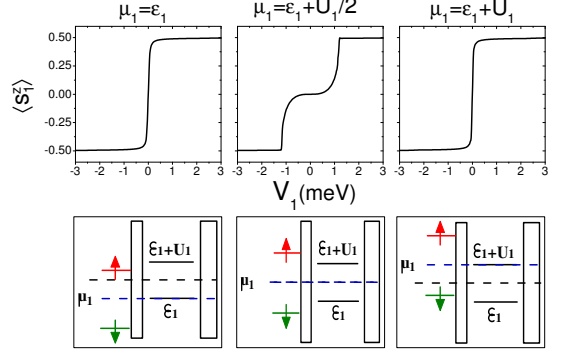


FIG. 4:  $\langle s_1^z \rangle$  vs  $V_1$  when  $\mu_1$  is aligned with  $\epsilon_1$ ,  $\epsilon_1 + U_1/2$ , and  $\epsilon_1 + U_1$ . Notice that for the first and the last cases,  $\langle s_1^z \rangle$  is immediately reversed between  $\sim 1/2$  and  $\sim -1/2$  when spin bias  $V_1$  is changed from positive to negative over a width  $\sim \Gamma_1$ .

are very sharp because  $\Gamma_1$  is much smaller than  $U_1$ . Increasing dot-lead coupling will blur the edges, and lower the efficiency of manipulation. Moreover, as shown in Fig. 4, at two conditions when  $\mu_1$  is aligned with  $\epsilon_1$ , or  $\epsilon_1 + U_1$ , the maximal polarization can be achieved immediately as long as the spin bias  $V_1$  overwhelms  $\Gamma_1$ , the broadening of dot level due to dot-lead coupling. In both situations there is only one electron in dot. So if dot is weakly coupled to the leads, one can manipulate the single spin by using a small spin bias.  $\mu_1 = \epsilon_1 + U_1/2$  in Fig.4 represents the hardest condition to polarize the spin, in which the spin bias has to overcome the intradot Coulomb repulsion energy.

#### IV. MEASUREMENT OF QUANTUM SPIN BY MEANS OF SPIN BIAS

In this section, the calculation and numerical results on the transport through dot 2 in the presence of a small spin bias  $V_2$  is presented, and its relation with the spin orientation in dot 1 is illustrated in details.

##### A. Effective field approximation

Based on Eqs. (1) and (2), when calculating the physical quantities of dot 2, the self-consistency for those of dot 1 can be ignored. In this limit, we treat the spin of dot 1 as an effective magnetic field using the Hamiltonian

$$V'_{12} = \frac{J}{2} s_1^- d_{2\uparrow}^\dagger d_{2\downarrow} + \frac{J}{2} s_1^+ d_{2\downarrow}^\dagger d_{2\uparrow} + \frac{J}{2} s_1^z (n_{2\uparrow} - n_{2\downarrow}), \quad (6)$$

where  $s_1^{\pm, z}$  are quantum field operators. It is worth stressing that the self-consistent calculation is very complicated, but still available in the present problem. To avoid mathematics, the present approximation is believed to give an intuitive picture of how the spin bias is converted into a charge signal.

## B. Spin-dependent transport and Green's function technique

In Sec. II A, we have made it clear that the direction of the net charge current that can flow through dot 2 in the presence of a small spin bias  $V_2$  can be used to detect the spin orientation in dot 1. Thus, it is convenient to introduce a quantity spin conductance, which is defined as the ratio of the charge current to the spin bias in the limit of the zero spin bias.<sup>36</sup> In Appendix A, we derive the formula of spin conductance at zero temperature,

$$G^s(\mu) = \lim_{V^s \rightarrow 0} \frac{\partial(I_\uparrow + I_\downarrow)}{\partial V^s} = \frac{e^2}{h} [T_\uparrow(\mu) - T_\downarrow(\mu)], \quad (7)$$

where  $T_{2\sigma}$  is the transmission probability for  $\sigma$  electrons through dot 2 within the framework of linear response theory. Therefore, the numerical results presented in Secs. IV C and IV D are given only in terms of  $T_{2\uparrow} - T_{2\downarrow}$  in the unit of  $\frac{e^2}{h}$ .

In the linear response theory, the  $\sigma$  component of the transmission probability is given by<sup>50</sup>

$$T_{2\sigma}(\mu_2) = [G_{2\sigma}^r(\omega)\Gamma_2^L(G_{2\sigma}^r(\omega))^\dagger\Gamma_2^R]_{\omega=\mu_2},$$

where the retarded Green's function  $G_2^r(\omega)$  is defined as the Fourier transform of

$$G_{2\sigma}^r(t) = -i\theta(t)\langle\{d_{2\sigma}(t), d_{2\sigma}^\dagger\}\rangle$$

with  $d_{2\sigma}(t) = e^{i(H_2+V_{12})t}d_{2\sigma}e^{-i(H_2+V_{12})t}$ .  $\Gamma_2^\alpha = \sum_k 2\pi|V_{k\alpha\sigma}|^2 2\pi\delta(\omega - \epsilon_{k\alpha\sigma})$  is the broadening of dot 2 level  $\epsilon_2$  due to the couplings to the  $\alpha$  lead. Using the equation of motion of  $G_{2\sigma}^r$  with respect to  $H_2 + V_{12}^r$ , we arrive at (detailed deductions and approximations are given in Appendix B)

$$\begin{pmatrix} \Omega & -\frac{J}{2} & -\frac{J}{2} \\ -\frac{J}{8} & \Omega & \frac{J}{4} \\ -\frac{J}{4} & \frac{J}{2} & \Omega + \frac{J}{4} \end{pmatrix} \begin{pmatrix} G_{2\uparrow}^r \\ G_2 \\ G_3 \end{pmatrix} = \begin{pmatrix} 1 + UG_4 \\ \langle s_1^z \rangle + UG_5 + \frac{J}{2}G_6 \\ JG_5 + \frac{J+2U}{2}G_6 \end{pmatrix},$$

$$\begin{pmatrix} \Omega - U & -\frac{J}{2} & -\frac{J}{2} \\ -\frac{J}{8} & \Omega - U & -\frac{J}{4} \\ -\frac{J}{4} & -\frac{J}{2} & \Omega - \frac{J+4U}{4} \end{pmatrix} \begin{pmatrix} G_4 \\ G_5 \\ G_6 \end{pmatrix} = \begin{pmatrix} N_1 \\ N_2 \\ N_3 \end{pmatrix},$$

$$\begin{pmatrix} \Omega & \frac{J}{2} & -\frac{J}{2} \\ \frac{J}{8} & \Omega & -\frac{J}{4} \\ -\frac{J}{4} & -\frac{J}{2} & \Omega + \frac{J}{4} \end{pmatrix} \begin{pmatrix} G_{2\downarrow}^r \\ G_8 \\ G_9 \end{pmatrix} = \begin{pmatrix} 1 + UG_{10} \\ \langle s_1^z \rangle + UG_{11} - \frac{J}{2}G_{12} \\ -JG_{11} + \frac{J+2U}{2}G_{12} \end{pmatrix},$$

$$\begin{pmatrix} \Omega - U & \frac{J}{2} & -\frac{J}{2} \\ \frac{J}{8} & \Omega - U & \frac{J}{4} \\ -\frac{J}{4} & \frac{J}{2} & \Omega - \frac{J+4U}{4} \end{pmatrix} \begin{pmatrix} G_{10} \\ G_{11} \\ G_{12} \end{pmatrix} = \begin{pmatrix} N_4 \\ N_5 \\ N_6 \end{pmatrix}, \quad (8)$$

where we denote  $\Omega = \omega - \epsilon_2 + \frac{i}{2}\Gamma_2$ , and  $\Gamma_2 = \Gamma_2^L + \Gamma_2^R$ .  $G_2 = \langle\langle d_{2\uparrow}s_1^z|d_{2\uparrow}^\dagger \rangle\rangle$ ,  $G_3 = \langle\langle d_{2\downarrow}s_1^-|d_{2\uparrow}^\dagger \rangle\rangle$ ,  $G_4 = \langle\langle d_{2\uparrow}n_{2\downarrow}|d_{2\uparrow}^\dagger \rangle\rangle$ ,  $G_5 = \langle\langle d_{2\uparrow}n_{2\downarrow}s_1^z|d_{2\uparrow}^\dagger \rangle\rangle$ ,  $G_6 = \langle\langle d_{2\downarrow}n_{2\uparrow}s_1^-|d_{2\uparrow}^\dagger \rangle\rangle$ ,  $G_8 = \langle\langle d_{2\downarrow}s_1^z|d_{2\downarrow}^\dagger \rangle\rangle$ ,  $G_9 = \langle\langle d_{2\uparrow}s_1^+|d_{2\downarrow}^\dagger \rangle\rangle$ ,  $G_{10} = \langle\langle d_{2\downarrow}n_{2\uparrow}|d_{2\downarrow}^\dagger \rangle\rangle$ ,

$G_{11} = \langle\langle d_{2\downarrow}n_{2\uparrow}s_1^z|d_{2\downarrow}^\dagger \rangle\rangle$ , and  $G_{12} = \langle\langle d_{2\uparrow}n_{2\downarrow}s_1^+|d_{2\downarrow}^\dagger \rangle\rangle$ , where the notation  $\langle\langle A|B \rangle\rangle$  stands for the Fourier transform of the retarded Green's function  $-i\theta(t)\langle\{A(t), B\}\rangle$ .  $N_1 = \langle n_{2\downarrow} \rangle$ ,  $N_2 = \langle n_{2\downarrow}s_1^z \rangle$ ,  $N_3 = -\langle d_{2\uparrow}^\dagger d_{2\downarrow}s_1^- \rangle$ ,  $N_4 = \langle n_{2\uparrow} \rangle$ ,  $N_5 = \langle n_{2\uparrow}s_1^z \rangle$ , and  $N_6 = -\langle d_{2\downarrow}^\dagger d_{2\uparrow}s_1^+ \rangle$ . It is worth pointing out that our deduction is similar to that in a previous work,<sup>51</sup> however, our calculation retains  $\langle s_1^z \rangle$  as an input parameter ranging from -0.5 to 0.5, reflecting the spin polarization in dot 1 to be detected.

Using the identity of Green's functions at equilibrium,<sup>48,49</sup>

$$G^< = i\mathbf{A}f, \quad \mathbf{A} = -2\text{Im}G^r,$$

where  $\mathbf{A}$  is the spectral function. We self-consistently calculate the expectation values in Eq. (8), for example,

$$\begin{aligned} \langle d_{2\uparrow}^\dagger d_{2\downarrow}s_1^- \rangle &= -i\langle\langle d_{2\downarrow}(t)s_1^-(t)|d_{2\uparrow}^\dagger(t') \rangle\rangle_{t=t'}^< \\ &= -i \int \frac{d\omega}{2\pi} \langle\langle d_{2\downarrow}s_1^-|d_{2\uparrow}^\dagger \rangle\rangle_\omega^< \\ &= -\frac{1}{\pi} \int d\omega f_2(\omega) \text{Im}\langle\langle d_{2\downarrow}s_1^-|d_{2\uparrow}^\dagger \rangle\rangle, \quad (9) \end{aligned}$$

where

$$f_2 = \frac{1}{e^{(\omega-\mu_2)/k_B T} + 1}.$$

## C. Numerical results

For numerical calculations, we choose a set of parameters consistent with the parallel-coupled double-quantum-dot experiment by Chen *et al.*,<sup>42</sup>  $k_B T = 0.004$  meV,  $J = 0.09$  meV,  $U_2 = 0.8$  meV, and  $\Gamma_2^\alpha = 0.0375$  meV. We set  $\epsilon_2 = -0.4$  meV to assure that  $\epsilon_1 + U_1/2 = \epsilon_2 + U_2/2$  is the zero point of energy. Despite the fact that the above experiment parameters lead to the Kondo effect at low temperatures,<sup>42</sup> we have enough reasons to rule it out from the present considerations. For dot 1, the spin is polarized by the large spin bias  $V_1$ ; thus, Kondo effect is usually quenched. For the dot 2, later we will see that the results are meaningful only when  $\mu_2$  is around the  $\epsilon_2$  and  $\epsilon_2 + U_2$ , where the first-order tunneling between leads L2 and R2 through dot 2 is dominant and suppresses the Kondo effect.

We assume that there is an unknown spin in dot 1 to be detected, i.e., all the  $\mathbf{S}$  regimes in Fig. 3. The states of dot 2 and the double-dot are classified by the electron occupation, and are shown with their energies in Table II for  $J > 0$ . The one-electron state of the double-dot is also the empty state (0) of dot 2. The doubly occupied states (D) of dot 2 are two-fold degenerate triply occupied states of the double-dot. The singly occupied state of the dot 2, due to the exchange interaction, could favor parallel (P) or antiparallel (AP) alignment with the spin in dot 1.

The poles of Green's functions of dot 2 reflect the energies required for transitions between these states with different occupancies of electrons. When the Fermi surface of leads are aligned with these poles and supply the required energy, the transitions will take place, giving rise to a conductance

TABLE II: The energy spectrum of dot 2 for  $J > 0$  when assuming there is an electron in dot 1, where P or AP corresponds, respectively, to the situation where parallel or antiparallel alignment of two spins is favored. One just exchanges the antiparallel and parallel alignments to have the  $J < 0$  case.

electron number in double-dot	1	2	3
electron number in dot 2	0	1	2
Ground state	Empty(0) $E_0 = 0$	Anti-parallel(AP) $E_1^{\text{AP}} = \epsilon_2 - \frac{3}{4}J$	Double(D) $E_2 = 2\epsilon_2 + U_2$
Excited states		Parallel(P) $E_1^{\text{P}} = \epsilon_2 + \frac{1}{4}J$	

peak. We list the four possible transitions to fill dot 2 with  $0 \rightarrow 1 \rightarrow 2$  electrons when  $J > 0$  in Table III, together with the energies required by the transitions and the corresponding charge conductance peaks in Fig. 5.

TABLE III: Transitions between states with different particle numbers in the dot 2 when  $J > 0$ , energies required from the Fermi surface to supply the transitions, and the corresponding conductance peaks in Fig. 5.

Transitions	Required energies	Peaks in Fig. 5
$0 \rightarrow \text{AP}$	$E_1^{\text{AP}} - E_0 = \epsilon_2 - \frac{3}{4}J$	1 (left)
$0 \rightarrow \text{P}$	$E_1^{\text{P}} - E_0 = \epsilon_2 + \frac{1}{4}J$	2
$\text{P} \rightarrow \text{D}$	$E_2 - E_1^{\text{P}} = \epsilon_2 + U_2 - \frac{1}{4}J$	3
$\text{AP} \rightarrow \text{D}$	$E_2 - E_1^{\text{AP}} = \epsilon_2 + U_2 + \frac{3}{4}J$	4 (right)

There are four charge conductance peaks in Fig. 5, forming two groups spaced by  $U_2$ . The peaks in each group are separated by  $J$ . When  $\langle s_1^z \rangle = 0$ , the numerical results are in good agreement with those by Tolea and Bulka.<sup>51</sup> From the above results, one understands why we ignore the inter-dot capacitive repulsion  $U'n_1n_2$ . In the singly occupied regime of dot 1, this term adds  $U'$  to the singly occupied energy and  $2U'$  to the doubly occupied energy of dot 2, so it only widens the spacing between peaks 1 and 2 with respect to peaks 3 and 4 by  $U'$  in the conductance spectrum of dot 2 and does not contribute to any spin-dependent effect.

Interesting results emerge when  $\langle s_1^z \rangle \neq 0$ . As an example, we consider the case  $\langle s_1^z \rangle > 0$ ; i.e., an  $\uparrow$  electron is in dot 1. We start with the empty state of the dot 2; i.e.,  $\mu_2$  is well below the energy of  $0 \rightarrow \text{AP}$  transition at  $\epsilon_2 - 3J/4$ . When  $\mu_2$  is raised to be aligned with the transition pole  $0 \rightarrow \text{AP}$ , dot 2 will favor  $\downarrow$  electron occupation because of the  $\uparrow$  electron in the dot 1. As shown in Fig. 6, the difference  $(n_{2\downarrow} - n_{2\uparrow})$  and  $\langle s_2^z \rangle$  reach maximum after  $\mu_2$  is above the transition  $0 \rightarrow \text{AP}$  at  $\epsilon_2 - 3J/4$ . The transport of  $\downarrow$  ( $\uparrow$ ) electrons through dot 2 via  $0 \rightarrow \text{AP}$  thus will be enhanced (suppressed), i.e.,  $T_{2\uparrow} - T_{2\downarrow} < 0$ , which accounts for the negative value region around  $\epsilon_2 - 3J/4$  (transition  $0 \rightarrow \text{AP}$ ) in Fig. 6 when  $\langle s_1^z \rangle > 0$ . When raising of  $\mu_2$  is continued until it is aligned with the transition  $0 \rightarrow \text{P}$  at  $\epsilon_2 + J/4$ , the electron in dot 2 could be either  $\uparrow$  or  $\downarrow$  because both situations are energetically allowed. A direct result of this nearly arbitrary spin polarization is that the second electron added to dot

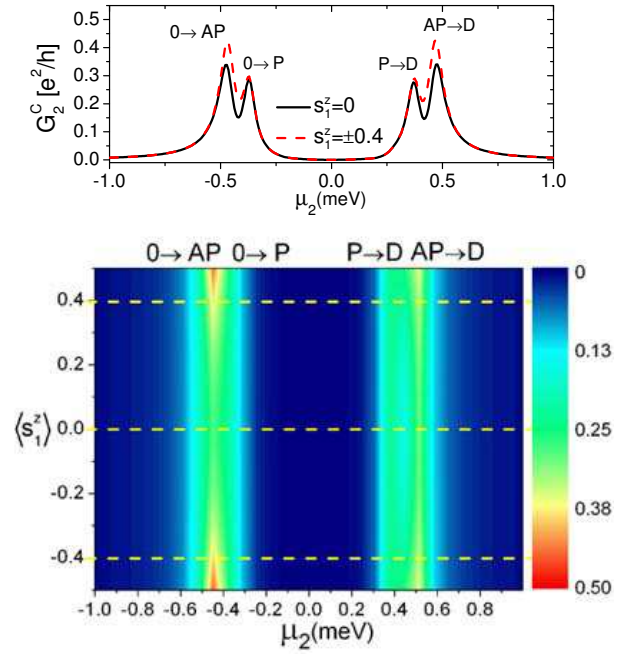


FIG. 5: The charge conductance ( $\frac{e^2}{h}(T_{2\uparrow} + T_{2\downarrow})$ ) vs  $\mu_2$  and  $\langle s_1^z \rangle$ .  $\mu_2$  is the equilibrium Fermi level. The exchange coupling strength  $J = 0.09$  meV,  $U_2 = 0.8$  meV,  $\epsilon_2 = -0.4$  meV, and  $\Gamma_2^g = 0.0375$  meV. The upper panel shows the values along the horizontal dashed lines in the lower panel.

2 via the transition  $\text{P} \rightarrow \text{D}$  can also be either  $\uparrow$  or  $\downarrow$ . Thus, no spin orientation is particularly favored when electrons tunnel via the transitions  $0 \rightarrow \text{P}$  at  $\epsilon_2 + \frac{1}{4}J$  and  $\text{P} \rightarrow \text{D}$  at  $\epsilon_2 + U_2 - \frac{1}{4}J$ . As a result,  $n_{2\downarrow} - n_{2\uparrow}$  approaches zero between  $\epsilon_2 + \frac{1}{4}J$  and  $\epsilon_2 + U_2 - \frac{1}{4}J$ , and there is only an invisible difference between  $T_{2\uparrow}$  and  $T_{2\downarrow}$  at both energies. If the second electron is added via the transition  $\text{AP} \rightarrow \text{D}$  at  $\epsilon_2 + U_2 + \frac{3}{4}J$ , it will automatically favor  $\uparrow$  because there is already a  $\downarrow$  electron in dot 2. This process is clearly shown as  $n_{2\downarrow} - n_{2\uparrow}$  reaches a maximum between  $\epsilon_2 + U_2 - \frac{1}{4}J < \mu_2 < \epsilon_2 + U_2 + \frac{3}{4}J$  and finally goes to zero after  $\mu_2 > \epsilon_2 + U_2 + \frac{3}{4}J$ . Hence,  $T_{2\uparrow} - T_{2\downarrow} > 0$  when  $\mu_2$  is aligned with the transition  $\text{AP} \rightarrow \text{D}$  at  $\epsilon_2 + U_2 + \frac{3}{4}J$ .

By the same token, the case  $\langle s_1^z \rangle < 0$  can be calculated. In Fig. 7, we compare the charge and spin conductances as functions of  $\langle s_1^z \rangle$  at  $\mu_2 = \epsilon_2 - 3J/4$  ( $0 \rightarrow \text{AP}$ ) and  $\epsilon_2 + J/4$  ( $0 \rightarrow \text{P}$ ). The major difference is that at  $0 \rightarrow \text{AP}$ ,  $T_{2\uparrow} - T_{2\downarrow}$  changes sign as  $\langle s_1^z \rangle$  turns from positive to negative polarization, while  $T_{2\uparrow} + T_{2\downarrow}$  remains positive. Therefore, the spin conductance of dot 2 provides a practical tool to probe the spin polarization in dot 1.

#### D. Model study when $J < 0$

The case of  $J < 0$  is different from that of  $J > 0$  because in this situation the ground states favors the parallel alignment of two spins in the two dots. Since there are no corresponding experiment data for  $J < 0$ , we just assume a set of model



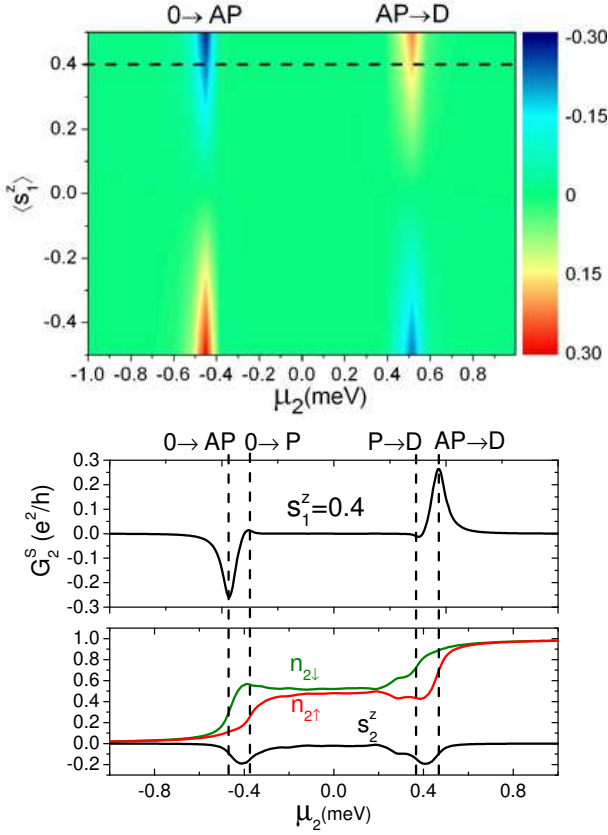


FIG. 6: The spin conductance ( $\frac{e^2}{h}(T_{2\uparrow} - T_{2\downarrow})$ ) vs  $\mu_2$  and  $\langle s_1^z \rangle$ .  $\mu_2$  is the equilibrium Fermi level. The parameters are the same as those in Fig. 5. The lower panel shows the values along the horizontal dashed line in the higher panel.

parameters in analogy to those when  $J > 0$ . In the charge conductance  $\mathcal{G}_2^C$  in Fig. 8, only two peaks are clearly visible; they come from the transitions  $0 \rightarrow P$  and  $P \rightarrow D$ . The conductance peaks for  $0 \rightarrow AP$  and  $AP \rightarrow D$  are suppressed. Unlike the P states, which actually originate from the three-fold triplets when  $s_1^z = 0$ , there is only one AP state. The contribution of AP to conductance as an excited state is too weak compared to those of P states, in particular, as dot 2 is weakly coupled to the leads.<sup>51</sup> As we see in Fig. 5, the peak maximum of the AP state as the ground state and the total three P states as the excited states are roughly of the same order, so the peak maximum of  $0 \rightarrow AP$  in  $\mathcal{G}_2^C$  of Fig. 8 as the excited state should be about 1 order ( $3 \times 3$ ) smaller than that of the P states as the ground state.

For the spin conductance  $\mathcal{G}_2^S$  in Fig. 8, two changes occur compared with that in Fig. 6. The first is that the peak and dip positions move to  $E_1^P - E_0 = \epsilon_2 + \frac{1}{4}J$  and  $E_2 - E_1^P = \epsilon_2 + U_2 - \frac{1}{4}J$ , because the P states are one-electron ground states for dot 2 when  $J < 0$ . The second is that the spin conductance changes sign with respect to that in Fig. 6 because the first electron that enters dot 2 tends to be parallel aligned with the spin in dot 1 when  $J < 0$ , in contrast to the anti-parallel alignment when  $J > 0$ .

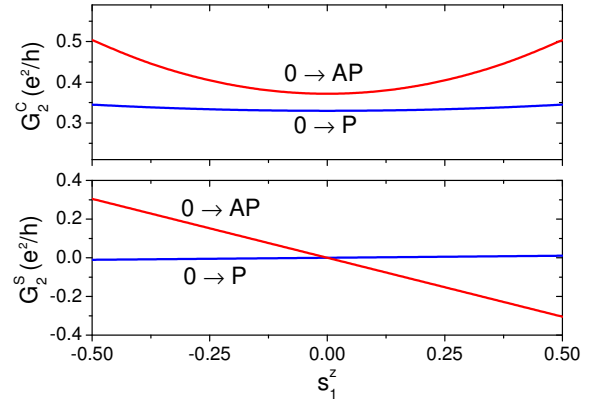


FIG. 7: The charge conductance ( $T_{2\uparrow} + T_{2\downarrow}$ ) and spin conductance ( $T_{2\uparrow} - T_{2\downarrow}$ ) vs  $\langle s_1^z \rangle$  when  $\mu_2 = \epsilon_2 - 3J/4$  ( $0 \rightarrow AP$ ) and  $\epsilon_2 + J/4$  ( $0 \rightarrow P$ ). The other parameters are the same as in Figs. 5 and 6.

## V. SUMMARY

We proposed a scheme to realize the control and detection of quantum spin in semiconductor quantum dot by means of spin bias or spin current. A double-quantum-dot system, coupled to electrodes with spin-dependent splitting of chemical potentials (spin bias), was investigated to demonstrate the availability of the proposal. Using a large spin bias, the quantum spin in dot 1 can be manipulated and maintained in a pure electric manner. The parameters and regimes of the manipulation were discussed in details. When an interdot exchange coupling is taken into account, the ground state of the two spins singly occupied in each dot tends to form an anti-parallel or a parallel alignment, depending on whether the coupling constant  $J$  positive or negative. The spin-dependent transport through dot 2 thus can be used to detect the polarization of spin in dot 1 nondestructively. We found that the measurement of the spin-dependent transport can be realized by measuring the net electric current under a spin bias, which defines a spin conductance. We observed that the spin conductance of dot 2 changes its sign as the orientation of spin in the dot 1 reverses, much more sensitively than the usual charge conductance does. The two cases demonstrate that the spin bias may be a promising approach to manipulate a single spin while allowing this manipulation to be monitored in quantum dot systems.

## VI. ACKNOWLEDGEMENTS

We thank Q. F. Sun, R. Lü, Y. J. Bao, B. Zhou, and R. B. Liu for discussions. This work was supported by the Research Grant Council of Hong Kong under Grant No. HKU 7041/07P.

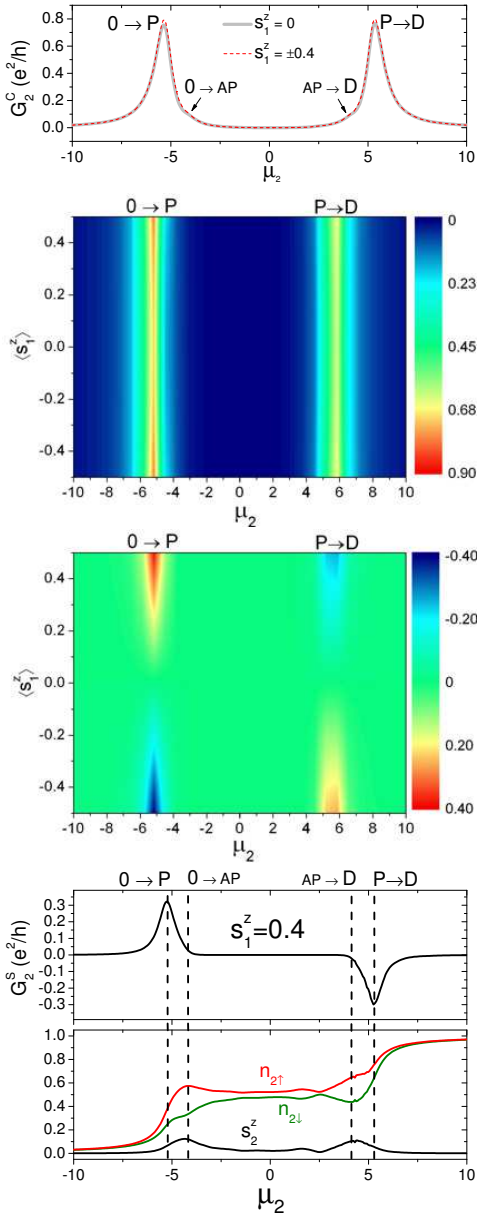


FIG. 8: The charge conductance [  $\frac{e^2}{h}(T_{2\uparrow} + T_{2\downarrow})$ , top two panels ] and the spin conductance [  $\frac{e^2}{h}(T_{2\uparrow} - T_{2\downarrow})$ , bottom two panels ] vs  $\mu_2$  and  $\langle s_1^z \rangle$  for negative exchange coupling  $J$ . The parameters are  $J = -1$ ,  $\epsilon_2 = -5$ ,  $U_2 = 10$ , and  $\Gamma_2 = 1$ .

#### APPENDIX A: THE FORMULA OF SPIN CONDUCTANCE

The conventional zero-bias differential conductance for spin component  $\sigma$  is defined as

$$\mathcal{G}_\sigma^c = \lim_{V^c \rightarrow 0} \frac{\partial I_\sigma}{\partial V^c} = -\frac{e}{h} \lim_{V^c \rightarrow 0} \frac{\partial}{\partial V^c} \int d\omega (f_L - f_R) T_\sigma(\omega),$$

where without loss of generality the charge bias  $V^c$  is assumed to change only the Fermi level of the left lead,

$$f_L = \frac{1}{e^{(\omega - \mu + eV^c)/k_B T} + 1}, f_R = \frac{1}{e^{(\omega - \mu)/k_B T} + 1}, \quad (\text{A1})$$

and  $\mu$  is the Fermi level of both leads when there is no bias. Supposing the transmission probability  $T_\sigma$  is not a function of the bias,

$$\mathcal{G}_\sigma^c = -\frac{e}{h} \int d\omega \left[ \frac{\partial f_L}{\partial V^c} \right]_{V^c \rightarrow 0} T_\sigma(\omega),$$

where  $\left[ \frac{\partial f_L}{\partial V^c} \right]_{V^c \rightarrow 0} \rightarrow -e\delta(\omega - \mu)$  when the temperature  $k_B T \rightarrow 0$ . Thus, at zero temperature, the total conductance including two spin components is

$$\mathcal{G}^c = \lim_{V^c \rightarrow 0} \frac{\partial(I_\uparrow + I_\downarrow)}{\partial V^c} = \sum_\sigma \mathcal{G}_\sigma^c = \frac{e^2}{h} [T_\uparrow(\mu) + T_\downarrow(\mu)].$$

If a spin bias  $V^s$  is applied so that  $\mu_\uparrow^L = \mu_\downarrow^R = \mu - eV^s/2$  and  $\mu_\downarrow^L = \mu_\uparrow^R = \mu + eV^s/2$ , and at zero temperature

$$\begin{aligned} \left[ \frac{\partial f_{L\uparrow}}{\partial V^s} \right]_{V^s \rightarrow 0} &= \left[ \frac{\partial f_{R\downarrow}}{\partial V^s} \right]_{V^s \rightarrow 0} \rightarrow -\frac{e}{2} \delta(\omega - \mu), \\ \left[ \frac{\partial f_{L\downarrow}}{\partial V^s} \right]_{V^s \rightarrow 0} &= \left[ \frac{\partial f_{R\uparrow}}{\partial V^s} \right]_{V^s \rightarrow 0} \rightarrow \frac{e}{2} \delta(\omega - \mu), \end{aligned} \quad (\text{A2})$$

then the differential conductance induced by the spin bias (or spin conductance for short) is defined as<sup>36</sup>

$$\mathcal{G}^s = \lim_{V^s \rightarrow 0} \frac{\partial(I_\uparrow + I_\downarrow)}{\partial V^s} = \frac{e^2}{h} [T_\uparrow(\mu) - T_\downarrow(\mu)], \quad (\text{A3})$$

which is proportional to the difference between the transmission probabilities of two spin components. The physical picture of this definition is very clear. Because spin  $\uparrow$  and  $\downarrow$  are under opposite biases,  $I_\uparrow$  and  $I_\downarrow$  tend to flow along opposite directions.  $|I_\uparrow|$  and  $|I_\downarrow|$  must be unequal to generate a net charge current, which is an experimentally measurable quantity. Note that  $|I_\uparrow|$  can be larger or smaller than  $|I_\downarrow|$ , depending on the ability of the dot in conducting electron with spin  $\uparrow$  and  $\downarrow$ . Therefore, the spin conductance can be either positive or negative. From Eq. (A3), one immediately realizes that if the spin symmetry of a mesoscopic system is broken, it can be probed by the spin conductance. Experimentally, one just applies a very small spin bias  $\Delta V^s$ , then measures the net charge current  $\Delta I$  (note that there is no need to measure the polarization of the current; instead, the measurement of current direction is required), and performs  $\Delta I / \Delta V^s$  to have an approximation of Eq. (A3).

#### APPENDIX B: DEDUCTION OF GREEN'S FUNCTIONS IN EQ. (8)

This part of calculation is inspired by the work by Tolea and Bulka,<sup>51</sup> in which an  $\langle S^z \rangle = 0$  ( $\langle s_1^z \rangle$  in our model) case was studied. The equation of motion for  $\langle\langle d_{2\uparrow} | d_{2\uparrow}^\dagger \rangle\rangle$  in the Fourier space is written as

$$\begin{aligned} &(\omega - \epsilon_2 + \frac{i}{2}\Gamma_2) \langle\langle d_{2\uparrow} | d_{2\uparrow}^\dagger \rangle\rangle \\ &= 1 + \frac{J}{2} \langle\langle d_{2\downarrow} s_1^- | d_{2\uparrow}^\dagger \rangle\rangle + \frac{J}{2} \langle\langle d_{2\uparrow} s_1^z | d_{2\uparrow}^\dagger \rangle\rangle \\ &\quad + U_2 \langle\langle d_{2\uparrow} n_{2\downarrow} | d_{2\uparrow}^\dagger \rangle\rangle, \end{aligned} \quad (\text{B1})$$

where and in the following we suppress all the  $r$  superscripts of the retarded Green's functions, and introduce the notation  $\langle\langle A|B\rangle\rangle$  as the Fourier transform of  $-i\theta(t)\langle\{A(t), B\}\rangle$ . Continue writing the equation of motion of Green's functions that contain only the operators  $d_{2\sigma}$ ,  $d_{2\sigma}^\dagger$ , and  $s_1^{\sigma,\pm}$  until no more new Green's function is produced,

$$\begin{aligned} & (\omega - \epsilon_2 + \frac{J}{4})\langle\langle d_{2\downarrow} s_1^- | d_{2\uparrow}^\dagger \rangle\rangle \\ &= \frac{J}{4}\langle\langle d_{2\uparrow} | d_{2\uparrow}^\dagger \rangle\rangle - \frac{J}{2}\langle\langle d_{2\uparrow} s_1^z | d_{2\uparrow}^\dagger \rangle\rangle \\ & \quad + J\langle\langle d_{2\uparrow} n_{2\downarrow} s_1^z | d_{2\uparrow}^\dagger \rangle\rangle \\ & \quad + (\frac{J}{2} + U_2)\langle\langle d_{2\downarrow} n_{2\uparrow} s_1^- | d_{2\uparrow}^\dagger \rangle\rangle \\ & \quad + \sum_{k,\alpha} V_{k\alpha\downarrow} \langle\langle c_{k\alpha\downarrow} s_1^- | d_{2\uparrow}^\dagger \rangle\rangle, \end{aligned} \quad (\text{B2})$$

$$\begin{aligned} & (\omega - \epsilon_2)\langle\langle d_{2\uparrow} s_1^z | d_{2\uparrow}^\dagger \rangle\rangle \\ &= \langle s_1^z \rangle + \frac{J}{8}\langle\langle d_{2\uparrow} | d_{2\uparrow}^\dagger \rangle\rangle - \frac{J}{4}\langle\langle d_{2\downarrow} s_1^- | d_{2\uparrow}^\dagger \rangle\rangle \\ & \quad + \frac{J}{2}\langle\langle d_{2\downarrow} n_{2\uparrow} s_1^- | d_{2\uparrow}^\dagger \rangle\rangle + U_2\langle\langle d_{2\uparrow} n_{2\downarrow} s_1^z | d_{2\uparrow}^\dagger \rangle\rangle \\ & \quad + \sum_{k,\alpha} V_{k\alpha\uparrow} \langle\langle c_{k\alpha\uparrow} s_1^z | d_{2\uparrow}^\dagger \rangle\rangle, \end{aligned} \quad (\text{B3})$$

$$\begin{aligned} & (\omega - \epsilon_2 - U_2)\langle\langle d_{2\uparrow} n_{2\downarrow} | d_{2\uparrow}^\dagger \rangle\rangle \\ &= \langle n_{2\downarrow} \rangle + \frac{J}{2}\langle\langle d_{2\downarrow} n_{2\uparrow} s_1^- | d_{2\uparrow}^\dagger \rangle\rangle + \frac{J}{2}\langle\langle d_{2\uparrow} n_{2\downarrow} s_1^z | d_{2\uparrow}^\dagger \rangle\rangle \\ & \quad + \sum_{k,\alpha} V_{k\alpha\downarrow} \langle\langle d_{2\uparrow} d_{2\downarrow}^\dagger c_{k\alpha\downarrow} | d_{2\uparrow}^\dagger \rangle\rangle \\ & \quad - \sum_{k,\alpha} V_{k\alpha\downarrow} \langle\langle d_{2\uparrow} c_{k\alpha\downarrow}^\dagger d_{2\downarrow} | d_{2\uparrow}^\dagger \rangle\rangle \\ & \quad + \sum_{k,\alpha} V_{k\alpha\uparrow} \langle\langle c_{k\alpha\uparrow} n_{2\downarrow} | d_{2\uparrow}^\dagger \rangle\rangle, \end{aligned} \quad (\text{B4})$$

$$\begin{aligned} & (\omega - \epsilon_2 - U_2)\langle\langle d_{2\uparrow} n_{2\downarrow} s_1^z | d_{2\uparrow}^\dagger \rangle\rangle \\ &= \langle n_{2\downarrow} s_1^z \rangle + \frac{J}{4}\langle\langle d_{2\downarrow} n_{2\uparrow} s_1^- | d_{2\uparrow}^\dagger \rangle\rangle + \frac{J}{8}\langle\langle d_{2\uparrow} n_{2\downarrow} | d_{2\uparrow}^\dagger \rangle\rangle \\ & \quad + \sum_{k,\alpha} V_{k\alpha\downarrow} \langle\langle d_{2\uparrow} d_{2\downarrow}^\dagger c_{k\alpha\downarrow} s_1^z | d_{2\uparrow}^\dagger \rangle\rangle \\ & \quad - \sum_{k,\alpha} V_{k\alpha\downarrow} \langle\langle d_{2\uparrow} c_{k\alpha\downarrow}^\dagger d_{2\downarrow} s_1^z | d_{2\uparrow}^\dagger \rangle\rangle \\ & \quad + \sum_{k,\alpha} V_{k\alpha\uparrow} \langle\langle c_{k\alpha\uparrow} n_{2\downarrow} s_1^z | d_{2\uparrow}^\dagger \rangle\rangle, \end{aligned} \quad (\text{B5})$$

$$\begin{aligned} & (\omega - \epsilon_2 - U_2 - \frac{J}{4})\langle\langle d_{2\downarrow} n_{2\uparrow} s_1^- | d_{2\uparrow}^\dagger \rangle\rangle \\ &= -\langle d_{2\uparrow}^\dagger d_{2\downarrow} s_1^- \rangle + \frac{J}{4}\langle\langle d_{2\uparrow} n_{2\downarrow} | d_{2\uparrow}^\dagger \rangle\rangle \\ & \quad + \frac{J}{2}\langle\langle d_{2\uparrow} n_{2\downarrow} s_1^z | d_{2\uparrow}^\dagger \rangle\rangle \\ & \quad - \sum_k V_{k\alpha\uparrow} \langle\langle d_{2\downarrow} c_{k\uparrow}^\dagger d_{2\uparrow} s_1^- | d_{2\uparrow}^\dagger \rangle\rangle \\ & \quad + \sum_k V_{k\alpha\uparrow} \langle\langle d_{2\downarrow} d_{2\uparrow}^\dagger c_{k\uparrow} s_1^- | d_{2\uparrow}^\dagger \rangle\rangle \\ & \quad + \sum_{k\alpha} V_{k\alpha\downarrow} \langle\langle c_{k\alpha\downarrow} n_{2\uparrow} s_1^- | d_{2\uparrow}^\dagger \rangle\rangle, \end{aligned} \quad (\text{B6})$$

where we have taken advantage of the single occupation of dot 1, i.e.,  $n_{1\uparrow} + n_{1\downarrow} = 1$ , so that

$$\begin{aligned} s_1^{z/+} s_1^{+/-} &= \pm \frac{1}{2} s_2^{\pm}, \quad s_1^{z/-} s_1^{-/+} = \mp \frac{1}{2} s_2^{\mp}, \\ s_1^{\pm} s_1^{\mp} &= \frac{1}{2} \pm s_1^z, \quad (s_1^z)^2 = \frac{1}{4}. \end{aligned} \quad (\text{B7})$$

Using the approximation scheme proposed by the previous authors to treat quantum dots weakly coupled to electrodes,<sup>51,52</sup>

$$\begin{aligned} \sum_{k\alpha} V_{k\alpha\uparrow} \langle\langle c_{k\alpha\uparrow} s_1^z | d_{2\uparrow}^\dagger \rangle\rangle &\approx -\frac{i}{2} \Gamma_2 \langle\langle d_{2\uparrow} s_1^z | d_{2\uparrow}^\dagger \rangle\rangle, \\ \sum_{k\alpha} V_{k\alpha\downarrow} \langle\langle c_{k\alpha\downarrow} s_1^- | d_{2\uparrow}^\dagger \rangle\rangle &\approx -\frac{i}{2} \Gamma_2 \langle\langle d_{2\downarrow} s_1^- | d_{2\uparrow}^\dagger \rangle\rangle, \\ \sum_{k\alpha} V_{k\alpha\uparrow} \langle\langle c_{k\alpha\uparrow} n_{2\downarrow} | d_{2\uparrow}^\dagger \rangle\rangle &\approx -\frac{i}{2} \Gamma_2 \langle\langle d_{2\uparrow} n_{2\downarrow} | d_{2\uparrow}^\dagger \rangle\rangle, \\ \sum_{k\alpha} V_{k\alpha\downarrow} \langle\langle c_{k\alpha\downarrow} n_{2\uparrow} s_1^- | d_{2\uparrow}^\dagger \rangle\rangle &\approx -\frac{i}{2} \Gamma_2 \langle\langle d_{2\downarrow} n_{2\uparrow} s_1^- | d_{2\uparrow}^\dagger \rangle\rangle, \\ \sum_{k\alpha} V_{k\alpha\uparrow} \langle\langle c_{k\alpha\uparrow} n_{2\downarrow} s_1^z | d_{2\uparrow}^\dagger \rangle\rangle &\approx -\frac{i}{2} \Gamma_2 \langle\langle d_{2\uparrow} n_{2\downarrow} s_1^z | d_{2\uparrow}^\dagger \rangle\rangle, \\ \sum_{k\alpha} V_{k\alpha\downarrow} \langle\langle c_{k\alpha\downarrow} n_{2\uparrow} s_1^z | d_{2\uparrow}^\dagger \rangle\rangle &\approx -\frac{i}{2} \Gamma_2 \langle\langle d_{2\downarrow} n_{2\uparrow} s_1^z | d_{2\uparrow}^\dagger \rangle\rangle, \end{aligned} \quad (\text{B8})$$

where  $\Gamma_2 = \Gamma_2^L + \Gamma_2^R$ . Moreover, simultaneous hopping in and out of the quantum dot are regarded to cancel each other,<sup>52</sup>

$$\begin{aligned} \langle\langle d_{2\uparrow} c_{k\alpha\downarrow}^\dagger d_{2\downarrow} | d_{2\uparrow}^\dagger \rangle\rangle &\approx \langle\langle d_{2\uparrow} d_{2\downarrow}^\dagger c_{k\alpha\downarrow} | d_{2\uparrow}^\dagger \rangle\rangle, \\ \langle\langle d_{2\uparrow} c_{k\alpha\downarrow}^\dagger d_{2\downarrow} s_1^z | d_{2\uparrow}^\dagger \rangle\rangle &\approx \langle\langle d_{2\uparrow} d_{2\downarrow}^\dagger c_{k\alpha\downarrow} s_1^z | d_{2\uparrow}^\dagger \rangle\rangle, \\ \langle\langle d_{2\downarrow} c_{k\alpha\uparrow}^\dagger d_{2\uparrow} s_1^- | d_{2\uparrow}^\dagger \rangle\rangle &\approx \langle\langle d_{2\downarrow} d_{2\uparrow}^\dagger c_{k\alpha\uparrow} s_1^- | d_{2\uparrow}^\dagger \rangle\rangle. \end{aligned} \quad (\text{B9})$$

The above approximations are valid only when the quantum dot is weakly coupled to the leads and for temperatures higher than the Kondo temperature. The advantage of the approximation is that it retains the full inter-dot correlations and gives a correct physical picture in the Coulomb blockade regime. After applying the truncation approximation, the equation of motion for the spin  $\uparrow$  retarded Green's function of dot 2 in the singly occupied regime of dot 1 can be obtained as Eq. (8). The equation of motion for  $\langle\langle d_{2\downarrow} | d_{2\downarrow}^\dagger \rangle\rangle$  can be obtained similarly.

- <sup>1</sup> D. Loss and D. P. DiVincenzo, Phys. Rev. A **57**, 120 (1998).
- <sup>2</sup> A. S. Bracker, E. A. Stinaff, D. Gammon, M. E. Ware, J. G. Tischler, A. Shabaev, A. L. Efros, D. Park, D. Gershoni, V. L. Korenev, et al., Phys. Rev. Lett. **94**, 047402 (2005).
- <sup>3</sup> A. Ebbens, D. N. Krizhanovskii, A. I. Tartakovskii, F. Pulizzi, T. Wright, A. V. Savelyev, M. S. Skolnick, and M. Hopkinson, Phys. Rev. B **72**, 073307 (2005).
- <sup>4</sup> T. H. Stievater, X. Li, T. Cubel, D. G. Steel, D. Gammon, D. S. Katzer, and D. Park, Appl. Phys. Lett. **81**, 4251 (2002).
- <sup>5</sup> X. Li, Y. Wu, D. G. Steel, D. Gammon, and L. J. Sham, Phys. Rev. B **70**, 195330 (2004).
- <sup>6</sup> A. Högele, M. Kroner, S. Seidl, K. Karrai, M. Atatüre, J. Dreiser, A. Imamoglu, R. J. Warburton, A. Badolato, B. D. Gerardot, et al., Appl. Phys. Lett. **86**, 221905 (2005).
- <sup>7</sup> D. Sprinzak, Y. Ji, M. Heiblum, D. Mahalu, and H. Shtrikman, Phys. Rev. Lett. **88**, 176805 (2002).
- <sup>8</sup> J. M. Elzerman, R. Hanson, J. S. Greidanus, L. H. W. van Beveren, S. DeFranceschi, L. M. K. Vandersypen, S. Tarucha, and L. P. Kouwenhoven, Phys. Rev. B **67**, 161308(R) (2003).
- <sup>9</sup> R. Hanson, L. Kouwenhoven, J. R. Petta, S. Tarucha, and L. M. K. Vandersypen, Rev. Mod. Phys. **79**, 1217 (2007).
- <sup>10</sup> F. H. L. Koppens, C. Buizert, K.-J. Tielrooij, I. T. Vink, K. C. Nowack, T. Meunier, L. P. Kouwenhoven, and L. M. K. Vandersypen, Nature(London) **442**, 766 (2006).
- <sup>11</sup> K. C. Nowack, F. H. L. Koppens, Y. V. Nazarov, and L. M. K. Vandersypen, Science **318**, 1430 (2007).
- <sup>12</sup> J. M. Elzerman, R. Hanson, L. H. W. van Beveren, B. Witkamp, L. M. K. Vandersypen, and L. P. Kouwenhoven, Nature (London) **430**, 431 (2004).
- <sup>13</sup> R. Hanson, L. H. W. van Beveren, I. T. Vink, J. M. Elzerman, W. J. M. Naber, F. L. Koppens, L. P. Kouwenhoven, and L. M. K. Vandersypen, Phys. Rev. Lett. **94**, 196802 (2005).
- <sup>14</sup> J. Berezovsky, M. H. Mikkelsen, O. Gywat, N. G. Stoltz, L. A. Coldren, and D. D. Awschalom, Science **314**, 1916 (2006).
- <sup>15</sup> J. Berezovsky, M. H. Mikkelsen, N. G. Stoltz, L. A. Coldren, and D. D. Awschalom, Science **320**, 349 (2008).
- <sup>16</sup> T. Meunier, I. T. Vink, L. H. W. van Beveren, F. H. L. Koppens, H. P. Tranitz, W. Wegscheider, L. P. Kouwenhoven, and L. M. K. Vandersypen, Phys. Rev. B **74**, 195303 (2006).
- <sup>17</sup> I. Zutic, J. Fabian, and S. D. Sarma, Rev. Mod. Phys. **76**, 323 (2004).
- <sup>18</sup> M. Johnson and R. H. Silsbee, Phys. Rev. Lett. **55**, 1790 (1985).
- <sup>19</sup> M. Johnson and R. H. Silsbee, Phys. Rev. Lett. **60**, 377 (1988).
- <sup>20</sup> S. O. Valenzuela and M. Tinkham, Nature (London) **442**, 176 (2006).
- <sup>21</sup> H. J. Zhu, M. Ramsteiner, H. Kostial, M. Wassermeier, H. P. Schönherr, and K. H. Ploog, Phys. Rev. Lett. **87**, 016601 (2001).
- <sup>22</sup> V. F. Motsnyi, J. D. Boeck, J. Das, W. V. Roy, G. Borghs, E. Goovaerts, and V. I. Safarov, Appl. Phys. Lett. **81**, 265 (2002).
- <sup>23</sup> A. T. Hanbicki, B. T. Jonker, G. Itskos, G. Kioseoglou, and A. Petrou, Appl. Phys. Lett. **80**, 1240 (2002).
- <sup>24</sup> R. Fiederling, M. Keim, G. Reuscher, W. Ossau, G. Schmidt, A. Waag, and L. W. Molenkamp, Nature (London) **402**, 787 (1999).
- <sup>25</sup> Y. Ohno, D. K. Young, B. Beschoten, F. Matsukura, H. Ohno, and D. D. Awschalom, Nature (London) **402**, 790 (1999).
- <sup>26</sup> Y. Kato, R. C. Myers, A. C. Gossard, and D. D. Awschalom, Science **306**, 1910 (2004).
- <sup>27</sup> J. Wunderlich, B. Kaestner, J. Sinova, and T. Jungwirth, Phys. Rev. Lett. **94**, 047204 (2005).
- <sup>28</sup> S. D. Ganichev, V. V. Bel'kov, S. A. Tarasenko, S. N. Danilov, S. Giglberger, C. Hoffmann, E. L. Ivchenko, D. Weiss, W. Wegscheider, C. Gerl, et al., Nature Physics **2**, 609 (2006).
- <sup>29</sup> X. D. Cui, S. Q. Shen, J. Li, Y. Ji, W. K. Ge, and F. C. Zhang, Appl. Phys. Lett. **90**, 242115 (2007).
- <sup>30</sup> J. Li, X. Dai, S.-Q. Shen, and F. C. Zhang, Appl. Phys. Lett. **88**, 162105 (2006).
- <sup>31</sup> L. L. Sohn, L. P. Kouwenhoven, and G. Schön, eds., *Mesoscopic Electron Transport, NATO Advanced Study Institutes, Ser. E*, vol. 345 (Kluwer, Dordrecht, 1997).
- <sup>32</sup> H. Park, J. Park, A. K. L. Lim, E. H. Anderson, A. P. Alivisatos, and P. L. McEuen, Nature (London) **407**, 57 (2000).
- <sup>33</sup> Y. Chye, M. E. White, E. Johnston-Halperin, B. D. Gerardot, D. D. Awschalom, and P. M. Petroff, Phys. Rev. B **66**, 201301(R) (2002).
- <sup>34</sup> M. Y. Veillette, C. Bena, and L. Balents, Phys. Rev. B **69**, 075319 (2004).
- <sup>35</sup> P. Zhang, Q.-K. Xue, and X. C. Xie, Phys. Rev. Lett. **91**, 196602 (2003).
- <sup>36</sup> D.-K. Wang, Q. F. Sun, and H. Guo, Phys. Rev. B **69**, 205312 (2004).
- <sup>37</sup> J. Li and S.-Q. Shen, Phys. Rev. B **76**, 153302 (2007).
- <sup>38</sup> Q. F. Sun, H. Guo, and J. Wang, Phys. Rev. Lett. **90**, 258301 (2003).
- <sup>39</sup> P. W. Anderson, Phys. Rev. **124**, 41 (1961).
- <sup>40</sup> A. W. Holleitner, C. R. Decker, H. Qin, K. Eberl, and R. H. Blick, Phys. Rev. Lett. **87**, 256802 (2001).
- <sup>41</sup> I. H. Chan, R. M. Westervelt, K. D. Maranowski, and A. C. Gosard, Appl. Phys. Lett. **80**, 1818 (2002).
- <sup>42</sup> J. C. Chen, A. M. Chang, and M. R. Melloch, Phys. Rev. Lett. **92**, 176801 (2004).
- <sup>43</sup> J. R. Petta, A. C. Johnson, J. M. Taylor, E. A. Laird, A. Yacoby, M. D. Lukin, C. M. Marcus, M. P. Hanson, and A. C. Gossard, Science **309**, 2180 (2005).
- <sup>44</sup> M. Zaffalon and B. J. van Wees, Phys. Rev. Lett. **91**, 186601 (2003).
- <sup>45</sup> P. Kotissek, M. Bailleul, M. Sperl, A. Spitzer, D. Schuh, W. Wegscheider, C. H. Back, and G. Bayreuther, Nature Physics **3**, 872 (2007).
- <sup>46</sup> S. O. Valenzuela and M. Tinkham, J. Appl. Phys. **101**, 09B103 (2007), and references therein.
- <sup>47</sup> N. C. van der Vaart, S. F. Godijn, Y. V. Nazarov, C. J. P. M. Harmans, and J. E. Mooij, Phys. Rev. Lett. **74**, 4702 (1995).
- <sup>48</sup> H. Haug and A.-P. Jauho, *Quantum Kinetics in Transport and Optics of Semiconductors* (Springer-Verlag, Berlin Heidelberg, 1996).
- <sup>49</sup> G. D. Mahan, *Many-Particle Physics* (Plenum Press, New York, 1990).
- <sup>50</sup> S. Datta, *Electronic Transport in Mesoscopic Systems* (Cambridge University Press, Cambridge, England, 1997).
- <sup>51</sup> M. Tolea and B. R. Bulka, Phys. Rev. B **75**, 125301 (2007).
- <sup>52</sup> B. R. Bulka and T. Kostyrko, Phys. Rev. B **70**, 205333 (2004).